Engineering 19 (2022) 24–39

Contents lists available at ScienceDirect

Engineering

journal homepage: www.elsevier.com/locate/eng

Research
Hydraulic Engineering—Article

Hydrological Response to Climate and Land Use Changes in the Dry–Warm Valley of the Upper Yangtze River

Congcong Li [a,c], Yanpeng Cai [b,d,*], Zhong Li [c], Qianqian Zhang [c,e], Lian Sun [a], Xinyi Li [c], Pengxiao Zhou [c]

[a] State Key Laboratory of Water Environment Simulation, School of Environment, Beijing Normal University, Beijing 100875, China
[b] Guangdong Provincial Key Laboratory of Water Quality Improvement and Ecological Restoration for Watersheds, Institute of Environmental and Ecological Engineering, Guangdong University of Technology, Guangzhou 510006, China
[c] Department of Civil Engineering, McMaster University, Hamilton, ON L8S 4L7, Canada
[d] Southern Marine Science and Engineering Guangdong Laboratory (Guangzhou), Guangzhou 511458, China
[e] Chengdu University of Information Technology, Chengdu 610225, China

ARTICLE INFO

Article history:
Received 4 June 2020
Revised 2 January 2021
Accepted 16 April 2021
Available online 20 October 2021

Keywords:
Dry–warm valley
Hydrologic simulation
Multi-ensemble GCMs
Climate change
Land use variations

ABSTRACT

The hydrological process in the dry–warm valley of the mountainous area of southwest China has unique characteristics and has attracted scientific attention worldwide. Given that this is an area with fragile ecosystems and intensive water resource conflicts in the upper reaches of the Yangtze River, a systematic identification of its hydrological responses to climate and land use variations needs to be performed. In this study, MIKE SHE was employed and calibrated for the Anning River Basin in the dry–warm valley. Subsequently, a deep learning neural network model of the long short-term memory (LSTM) and a traditional multi-model ensemble mean (MMEM) method were used for an ensemble of 31 global climate models (GCMs) for climate projection. The cellular automata–Markov model was implemented to project the spatial pattern of land use considering climatic, social, and economic conditions. Four sets of climate projections and three sets of land use projections were generated and fed into the MIKE SHE to project hydrologic responses from 2021 to 2050. For the calibration and first validation periods of the daily simulation, the coefficients of determination (R) were 0.85 and 0.87 and the Nash–Sutcliffe efficiency values were 0.72 and 0.73, respectively. The advanced LSTM performed better than the traditional MMEM method for daily temperature and monthly precipitation. The average monthly temperature projection under representative concentration pathway 8.5 (RCP8.5) was expected to be slightly higher than that under RCP4.5; this is contrary to the average monthly precipitation from June to October. The variations in streamflow and actual evapotranspiration (ET) were both more sensitive to climate change than to land use change. There was no significant relationship between the variations in streamflow and the ET in the study area. This work could provide general variation conditions and a range of hydrologic responses to complex and changing environments, thereby assisting with stochastic uncertainty and optimizing water resource management in critical regions.

1. Introduction

Changes in climatic conditions and land use patterns have been confirmed to have a significant influence on the spatial and temporal distribution of water resources within specific watersheds [1–3]. Such changes affect relevant hydrologic cycles by altering precipitation, evapotranspiration (ET), and the corresponding streamflow regimes [4], which potentially causes a reduction in water availability and an increase in water conflicts [5,6]. As noted above, many studies have been conducted to understand and analyze the hydrological cycles under climate change and human disturbance [1–7]. However, many challenges arise because of the complexities associated with certain hydrological cycles, particularly for the core process of the cycle, that is, streamflow. Generally, the identification and projection of relevant streamflow is considered an essential prerequisite for hydrologic cycle analysis. Streamflow projections under changing conditions are thus regarded as an important process that can contribute to water facility management, reservoir regulation, and water resource planning.

* Corresponding author.
E-mail address: yanpeng.cai@gdut.edu.cn (Y. Cai).

https://doi.org/10.1016/j.eng.2021.04.029

Consequently, identifying the dynamic characteristics of hydrological processes under climatic and land use variations are critical for evaluating the usability of water resources and developing adaptation strategies [8].

Previously, hydrologic models integrated with climatic and land use projections were adopted to evaluate the possible impacts of climate change on hydrological processes under multiple scenarios [9–11]. Wilby and Harris [12] evaluated the contribution of climatic factors to the dry seasonal phenomenon of the Thames watershed using two sets of parameters with four sets of global climate model (GCM) outputs and two hydrologic models under two emission scenarios. Ahiablame et al. [13] designed several scenarios of land use and climatic patterns to analyze the corresponding possible streamflow responses. Morán-Tejeda et al. [14] combined a regional climate model and multiple hypothetical land use scenarios with hydrologic models in a mountainous watershed. Several studies have also revealed that climate change is one of the dominant factors leading to streamflow variations [15]. The hydrologic models were commonly calibrated with historical data and then driven by future predictions of climate and land use variations for hydrologic studies. As the environmental changes are increasing significantly, it is predicted that future environmental factors will lead to dynamic changes in hydrological model parameters. Compared with indirect impacts of climate change on soil characteristics, land use variation has a much more significant impact by directly and quickly altering the soil porosity and connectivity [16]. As for land use variation, Merz et al. [17] pointed out that model parameters can be considered as fixed within five years, and Luo et al. [18] stated that hydrologic simulation should consider the different model parameters in different seasons, and then the indirect impact of land use change by changing the soil properties on the hydrologic process should be considered.

Generally, GCMs are widely used as primary tools for predicting future climatic changes. However, various uncertainties are associated with climate projections generated by GCMs owing to the complexity of climatic systems. The downscaling of GCMs to a suitable scale is frequently used to represent spatial heterogeneity [19]. Two common methods of dynamic and statistical downscaling are typically used for GCM projections [20]. Statistical downscaling aims to build statistical relations between historical GCMs and observations while there are adequate data, which have wide application in the related fields of hydrologic research [21–23]. The uncertainties [23,24] in hydrologic forecasting will increase because of the cumulative impacts of various options of multiple downscaling methods and GCMs. Multi-ensemble GCMs have been proven to be superior to an individual GCM, two methods such as long short-term memory (LSTM) and multi-model ensemble mean (MMEM) were usually adopted for ensembling GCMs [25–28]. There is little agreement on metrics to distinguish between "good" and "bad" models, and an ensemble of multiple climate models generally outperformed any individual model; this can improve the reliability and resolution of future climate projections [29–31]. Using machine learning models to ensemble or average multi-GCMs can reduce bias in projecting future hydrological responses [32].

Furthermore, there exist only a few models to project the land use variation because of the spatial characteristics and diversity of land use types. The current common methods include the cellular automata (CA) model, the Markov model, and the conversion of land use and its effects at small region extent (CLUE-S) model. The CLUE-S model has been widely used in small-scale applications, but there are limits on the number of types and grids [33]. The Markov model was primarily used to predict the temporal resolution, but it cannot present the spatial distribution of land use variations. This model is usually used along with other models to develop its advantages [34]. The CA model can identify the spatial dynamic evolution process for complex systems, but it is difficult to effectively reflect macro influences, such as social and economic factors. The CA–Markov model has a great advantage as it combines the powerful spatial computing ability of the CA model and the long-term prediction of the Markov model for spatial and temporal pattern stimulation, and is widely used for land use projections [35]. Moreover, the CA–Markov model contains the effects of natural, social, economic, administrative centers, transportation, and climate conditions on land use projections. However, most studies of the CA–Markov model have focused on large cities, and there are few studies on land use projection at the watershed scale, especially in mountainous areas.

The Anning River Basin (ARB) is a tributary of the upper Yangtze River and an ecotone of agricultural and animal husbandry. Because of its unique topography characterized by undulating terrain, high altitude, steep slopes, and valleys; the local ecosystem is inherently fragile. There exists an uneven seasonal and regional distribution of precipitation, strong storm intensity in the rainy period, little precipitation, and large ET in the dry season [36]. The climatic variation in the Yangtze River Basin has been analyzed in numerous previous studies using multiple methods and technologies [37]. An assessment of the hydrologic process under the combined influence of climate and land use should be conducted, particularly for fragile arid or semi-arid regions in the Yangtze River.

With the increase in complexity and uncertainty of changing conditions, the investigation and understanding of hydrological progress in ARB are challenging because of the following: ① the scarcity of hydrological modeling in a fragile region with complex terrains, ② finding an applicable technique for climatic projections among various scenarios, ③ spatial and temporal variations of land use for the future, and ④ diversity between simplified hydrologic models and nonlinear hydrologic processes [30]. It is a critical scientific issue that must be addressed immediately to consider the influencing factors of climate and land use under multiple spatial and temporal scales for long-term hydrologic forecasting in the dry–warm valley of the Yangtze River.

Therefore, the objectives of this research are ① to evaluate the feasibility of MIKE SHE in a mountainous area, ② to predict precipitation and temperature in the ARB with an ensemble of 31 GCMs to improve accuracy through LSTM and MMEM; ③ to explore land use projections in consideration of natural, social, and economic conditions, and ④ to investigate the underlying influence of climatic and land use variation on streamflow and actual ET. The developed model incorporated an ensemble of 31 GCMs for climate projections and a CA–Markov-based model for land use projections, which can not only resolve meteorological and land use projection uncertainties, but also investigate the dynamic variation condition and range of hydrologic processes. Consequently, this is of great significance in dealing with stochastic uncertainty and the optimization management of water resources under complex changing conditions. This work provides benchmarked information on adaptive measures for water resources and environmental sustainability in the upper Yangtze River for local and downstream areas.

2. Overview of the study site

The dry–warm valley in the Hengduan Mountain has a unique climatic, geographical, and hydrological features. It has a typical non-zonal climate, not only based on global climate change, but also closely related to local physical conditions. Zhang et al. [38] found that the climate in the dry–warm valley is inconsistent with global climate change; the temperature has declined since the 1950s, while the precipitation increased. As a typical potential ecological degradation region and an important agricultural

production base in China, hydrologic analysis under changing conditions is helpful for decision-making regarding development in the cropping system, biological resources, and ecological restoration.

The Anning River watershed, located in the dry–warm valley of southwest China, is a secondary tributary of the upper Yangtze River (Fig. 1). The range in latitude is between 102°06′E and 102°10′E and in longitude between 26°38′N and 29°02′N, with an elevation of 900–4750 m. It has a total length of 337 km and flows through Mianning, Xichang, Dechang, and Miyi, with a valley area of approximately 11 150 km^2. For several years, the average precipitation was 1240 mm, while the average temperature was 17–19 °C. There were distinct wet and dry seasons; the rainy season was from June to October and accounted for more than 90% of the annual rainfall. Intense rainfall, along with steep slopes and valleys, usually leads to flash floods. Alternatively, there is usually little precipitation and large evaporation during dry seasons. In both wet and dry seasons, precipitation exhibits significant spatial variability, with more rainfall in mountainous areas and less rainfall in the valleys.

As the mother river of Liangshan State, ARB is a gathering place for 14 national minorities. It is also the second-largest valley plain in Sichuan Province and an ecologically fragile region in the upper Yangtze River, which is a vital area for western economic development in China. Over the years, because of the influence of global climatic and land use variations, many eco-environmental problems, such as water shortages, land desertification, and water quality deterioration, have become serious obstacles to the development of ecological economics in southwest China. There are relatively concentrated social and economic activities, planning and construction of water conservancy and hydropower projects, large irrigation districts, and major cities, which have brought increasing uncertainties and difficulties to the system management of the watershed. Therefore, it is an urgent issue to analyze hydrologic responses of climate and land use variations for the rational use of water resources, constructing ecological barriers, and sustainable development for the Yangtze River.

3. Methodology

3.1. Integrated modeling framework

The main research objective is to project the hydrologic response to climate and land use variation using a hydrologic model. A flowchart of the hydrologic response projection is illustrated in Fig. 2. First, according to the availability and continuity of the meteorological and hydrological data, MIKE SHE was calibrated from 1977 to 1983 and validated from 1984 to 1986.

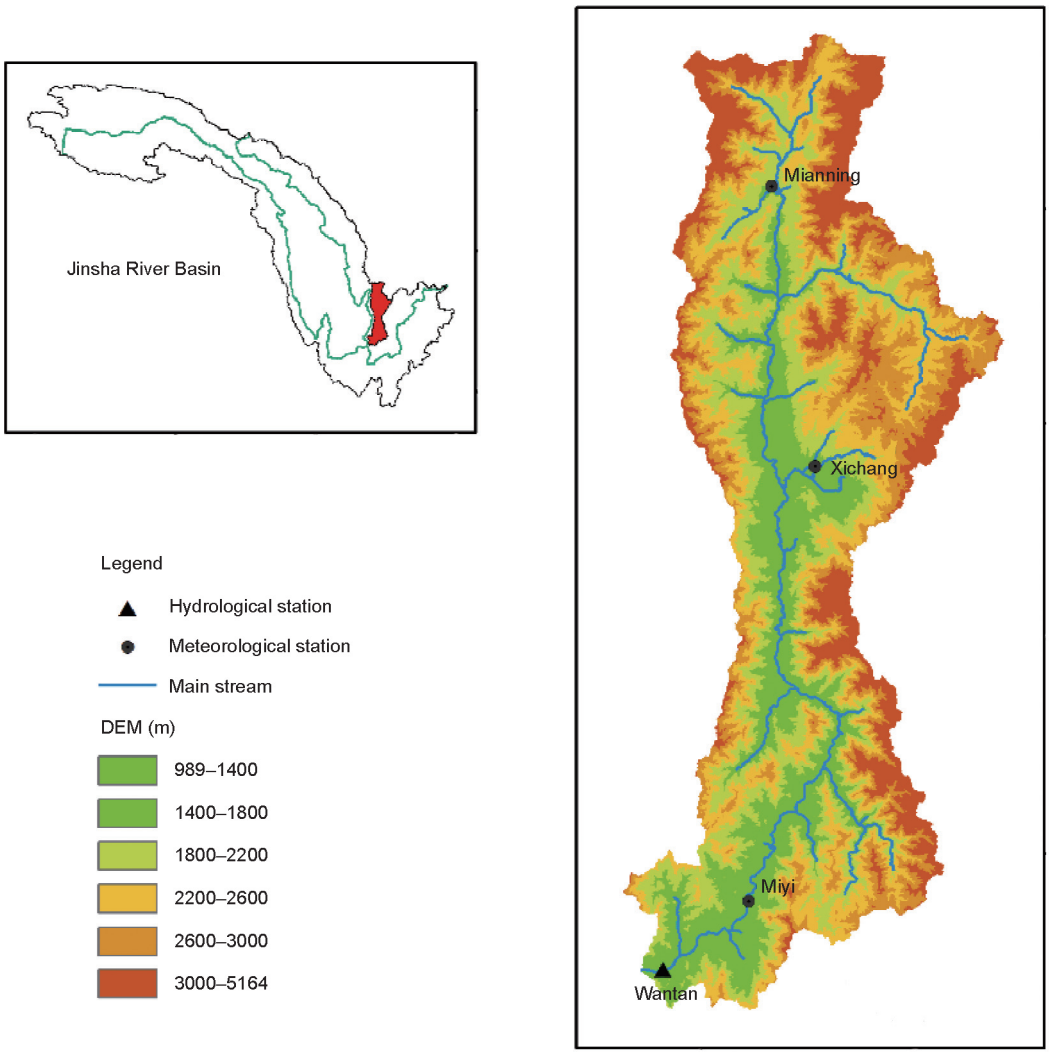

Fig. 1. The Anning River watershed. Jinsha River is the upper stream of Yangtze River. DEM: digital elevation model.

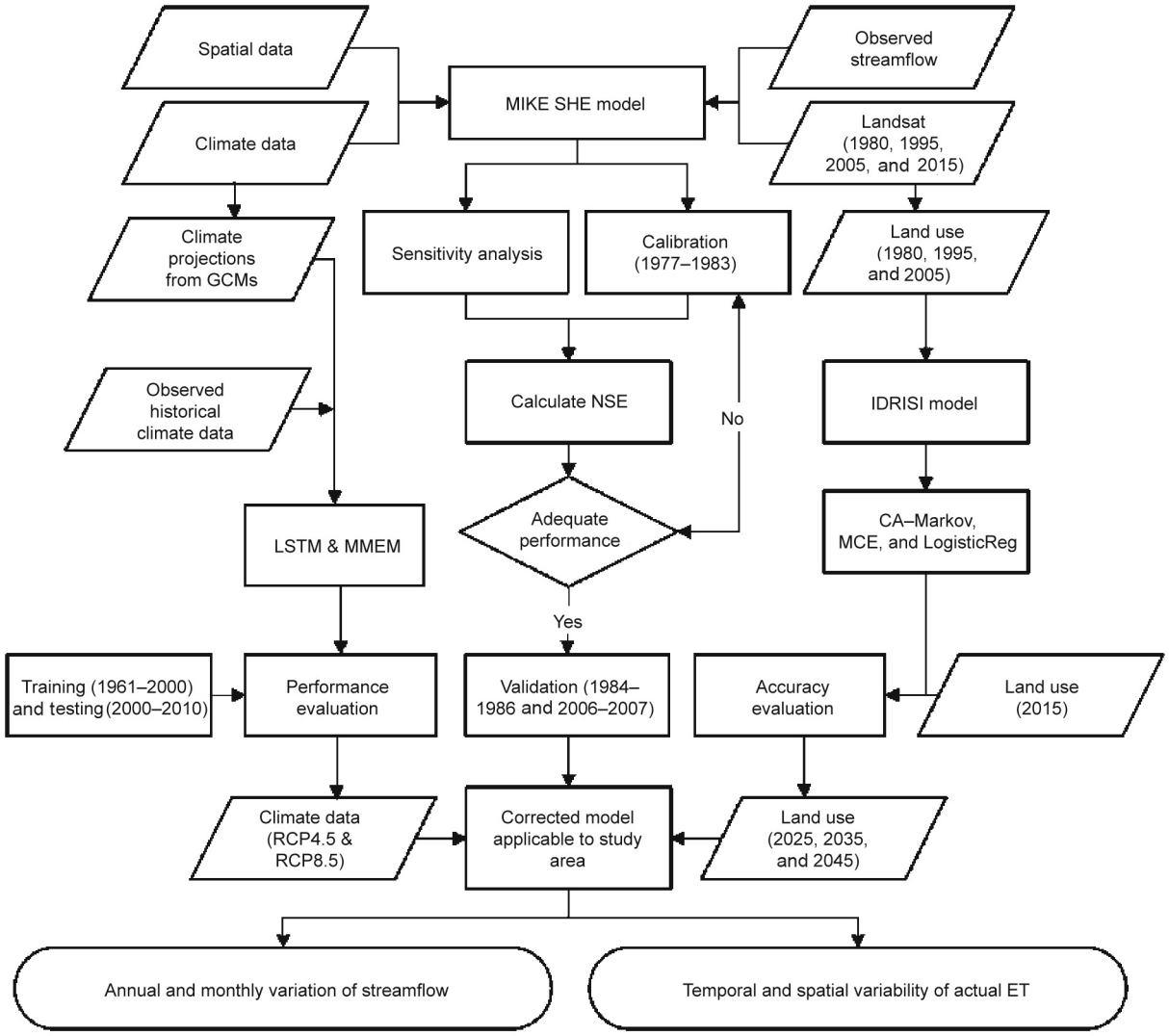

Fig. 2. Diagram for hydrologic response projection under climate and land use changes. NSE: Nash–Sutcliffe efficiency; RCP: representative concentration pathway; MCE: multi-criteria evaluation; LogisticReg: LogisticRegression.

Land use data from 1980 and the daily streamflow data at Wantan station were used for both calibration and validation. Subsequently, MIKE SHE was further validated from 2006 to 2007 with the land use data of 2005, and the sensitivity parameters remained unchanged, the performance of MIKE SHE remained well. Then, two climate ensembles of 31 GCMs based on LSTM and MMEM were developed to predict future climatic changes. The LSTM-based ensemble was trained using historical data from 1961 to 2000 and was tested using data from 2001 to 2010. Subsequently, the CA–Markov model combined with multi-criteria evaluation (MCE) and spatial multiple regression (LogisticReg) modules were used to project the three types of land use projections. Finally, we employed four sets of climate data projected by LSTM and MMEM and three sets of land use projections to drive MIKE SHE to evaluate future hydrologic responses in ARB.

3.2. Hydrologic modeling

A typical representative of the distributed hydrologic model based on the physical mechanism, MIKE SHE, was selected to explore the impacts of climate and land use changes on the hydrological process [39]. The model mainly considers hydrological processes such as plant interception, ET, overland flow, unsaturated and saturated zones, surface water, groundwater exchange, and snowmelt runoff, which can be estimated from the measured data as the parameters have physical significance [40]. The MIKE SHE model is mainly applied in the following four aspects: ① exploring the applicability of the model and the model construction process [41], ② parameter sensitivity analysis [42], calibration and verification [43], and model uncertainty analysis [44]; ③ feasibility analysis of constructing distributed hydrologic models in areas with insufficient data [45]; and ④ hydrologic responses to climatic and land use variation under the background of global warming [46]. MIKE SHE is a hydrologic model that has been universally used in multiple fields in numerous scales and has great application potential in humid and arid regions [47]. Additionally, researchers can choose suitable modules for modeling along with different climatic conditions, geological characteristics, and available data in the study region, which are different from the distributed hydrologic models such as the soil and water assessment tool (SWAT), variable infiltration capacity (VIC), and TOPMOEL [48].

3.2.1. Input data of hydrological model

The digital elevation model (DEM), meteorological, land use, soil, and hydrological data were used to characterize the spatial heterogeneity for hydrological modeling and analysis (Table 1).

Table 1
The input data for MIKE SHE model.

Data type	Name	Data Source
DEM	ASTER GDEM (30 m × 30 m)	GS Cloud
Climate data	Precipitation	National Meteorological Center
	Temperature	National Meteorological Center
	Reference evapotranspiration	Penman's equation
Vegetation	Land use map (30 m × 30 m)	Resource & Environment Cloud
	Leaf area index	FAO and field collection
	Root depth	FAO and field collection
Soil	Surface and sectional type (1 km × 1 km)	Harmonized World Soil Database
Hydrology	Streamflow	The People's Republic of China Hydrologic Yearbook

Three meteorological stations (Mianning, Xichang, and Miyi) located upstream of the outlet station were selected. The National Meteorological Center acquired downscale precipitation, high temperature, and low temperature-based stations from 1961 to 2010. The available Food and Agriculture Organization (FAO) Penman–Monteith method was used to evaluate the reference ET in this study [49]. Daily discharge observation values at the Wantan hydrologic station from the People's Republic of China Hydrologic Yearbook were used to calibrate and validate the MIKE SHE. DEM and land use data were acquired from the data platforms of the Chinese Academy of Sciences, whereas soil data were obtained from the Harmonized World Soil Database[†]. The Geographic Information System (GIS) tool was used to process and obtain spatial data information such as flow direction, flow concentration, drainage network, soil, and land use data in the study area.

Additionally, it is difficult for the static parameters of the hydrological model to reflect the changes in the hydrologic characteristics of the future environment. Vegetation coverage is one of the most critical environmental factors in the watershed, and it directly affects the distribution of rainfall between evaporation and runoff. For this study, the leaf area index (LAI) and root depth (RD) of vegetation were used as the characterization factors for the dynamic changes in model parameters, and the vegetation growth period and non-growth period were divided. Subsequently, based on climate change conditions such as precipitation and temperature, the functional relationship between LAI and RD was established and analyzed, and the dynamic parameters of LAI and RD for every decade in the future were estimated. The dynamic parameters of the hydrological model established the response relationship between the model parameters and vegetation changes.

3.2.2. Calibration and validation

The parameter calibration process adjusts the model to match the simulation results with the observed data. Over-parameterization occurs if all the parameters are freely adjusted during the calibration process. The primary sensitivity parameters are listed in Table 2, based on a literature review [50,51]. The auto calibration tool of the MIKE SHE model was adopted to calibrate the parameters (Table 2).

The Nash–Sutcliffe efficiency (NSE) coefficient and coefficient of determination (R) were used as statistical criteria to assess the MIKE SHE model performance in this study. The Nash–Sutcliffe coefficient is sensitive to both the mean and variance of the simulated and measured values. The coefficients of the NSE and R are as follows:

Table 2
Sensitive parameters of MIKE SHE for calibration.

Parameter	Initial value	Value range	Final value
Manning coefficient	20	5–50	25
Detention storage	2	0–20	4
Horizontal hydraulic conductivity	1.00×10^{-4}	1.00×10^{-5}–2.00×10^{-3}	1.25×10^{-3}
Vertical hydraulic conductivity	1.00×10^{-5}	1.00×10^{-6}–2.00×10^{-4}	1.25×10^{-4}
Specific yield	0.20	0.10–0.50	0.11
Storage coefficient	1.00×10^{-4}	1.00×10^{-7}–1.00×10^{-3}	2.22×10^{-5}
Drainage level	−0.5	−2.0–−0.1	−1.2
Time constant	1.00×10^{-6}	1.00×10^{-7}–1.00×10^{-5}	3.45×10^{-7}

$$\mathrm{NSE} = 1 - \sum_{i=1}^{n} (Q_m - Q_s)^2 / \sum_{i=1}^{n} (Q_m - \overline{Q_m})^2 \quad (1)$$

$$R = \sum_{i=1}^{n} (Q_m - \overline{Q_m}) \cdot (Q_s - \overline{Q_s}) / \sqrt{\sum_{i=1}^{n} (Q_m - \overline{Q_m})^2 \cdot \sum_{i=1}^{n} (Q_s - \overline{Q_s})^2} \quad (2)$$

where Q_m is the observation value, Q_s is the simulation value, and $\overline{Q_m}$ and $\overline{Q_s}$ are the average value of Q_m and Q_s, respectively. n represents the number of observation values (simulation values), and i represents the nth value.

The NSE value ranges from 0 to 1; the closer it is to 1, the better the simulation effect, and the higher the simulation accuracy. Generally, the model can be used for calculation when R of the simulated value and the measured value is greater than 0.6, and the simulation results reach a better level when the NSE value is between 0.50 and 0.95.

3.3. Multi-ensemble GCMs for climate projection

In this research, 31 GCMs at a monthly scale covering the time period 1961–2050 were downloaded from the Coupled Model Intercomparison Project Phase 5 (CMIP5) website[‡] (Table 3). The statistical downscaling model of a weather generator (NWAI-WG) developed by Liu and Zuo [52] was used to obtain data every day for each meteorological station. The dataset covers three variables: precipitation, maximum temperature, and minimum temperature. The Intergovernmental Panel on Climate Change 5 (IPCC5) report stated that greenhouse gas emissions are the main source of uncertainty for future temperature and precipitation. Representative concentration pathway 4.5 (RCP4.5) and RCP8.5 are moderate and higher mitigation scenarios, respectively, which are appropriate for research on the influence of climate [53].

Climate projections generated by GCMs are subject to significant uncertainties at large spatial scales and deviations in simulation. Multi-ensemble GCMs are generally considered superior to single models [54]. LSTM and MMEM methods were adopted for climate change projections to improve the prediction accuracy of the simulated outputs from multiple GCMs. MMEM is a traditional method that is evaluated using mean values from the multi-model ensemble. LSTM is a special type of recurrent neural network (RNN), capable of learning long-term dependencies and remembering information for long periods and has been proven to capture the temporal relationship among time series data better than traditional RNNs [26]. The introduction of LSTM was used to detect

[†] http://www.fao.org/soils-portal/data-hub/soil-maps-and-databases/harmonized-world-soil-database-v12/en/.

[‡] https://www.cesm.ucar.edu/experiments/cmip5.html.

Table 3
Basic information of 31 GCMs in CMIP5.

Model	Region	Resolution	Model	Region	Resolution
ACCESS1.0	Australia	1.87° × 1.25°	GISS-E2-R	The United States	2.50° × 2.00°
ACCESS1.3	Australia	1.87° × 1.25°	GFDL-CM3	The United States	2.50° × 2.00°
BCC-CSM1.1	China	2.80° × 2.80°	GFDL-ESM2G	The United States	2.50° × 2.00°
BCC-CSM1.1(m)	China	1.10° × 1.10°	GFDL-ESM2M	The United States	2.50° × 2.00°
BNU-ESM	China	2.80° × 2.80°	HadGEM2-AO	Republic of Korea	1.87° × 1.25°
CanESM2	Canada	2.80° × 2.80°	INM-CM4	Russia	2.00° × 1.50°
CCSM4	The United States	1.25° × 0.94°	IPSL-CM5A-MR	France	1.27° × 2.50°
CESM1(BGC)	The United States	1.25° × 0.94°	IPSL-CM5B-LR	France	1.89° × 3.75°
CESM1(CAM5)	The United States	1.25° × 0.94°	MIROC5	Japan	1.40° × 1.40°
CESM1(WACCM)	The United States	2.50° × 1.90°	MIROC-ESM	Japan	2.80° × 2.80°
CMCC-CM	Europe	0.75° × 0.75°	MPI-ESM-LR	Germany	1.87° × 1.86°
CMCC-CMS	Europe	1.86° × 1.87°	MRI-CGCM3	Japan	1.10° × 1.10°
EC-EARTH	Europe	1.10° × 1.10°	NorESM1-M	Norway	2.50° × 1.90°
FIO-ESM	China	2.80° × 2.80°	NorESM1-ME	Norway	2.50° × 1.90°
GISS-E2-H	The United States	2.50° × 2.00°	MIROC-ESM-CHEM	Japan	2.80° × 2.80°
GISS-E2-H-CC	The United States	2.50° × 2.00°			

temporal signals and build the nonlinearity correlation between downscaled data from the 31 GCMs and the observed data of the reference period, and then propagate the long-term information to a future period. The primary purpose of the LSTM was to integrate the GCM ensembles into high-quality and highly accurate precipitation and temperature.

The special structure of LSTM is that it has a memory cell, which is used to store information and propagate outputs for different time steps. A structure known as gates, which includes a forget gate, input gate, and output gate, manages the cell states and outputs. The gate consists of a sigmoid function with a multiplication operation. The sigmoid function varies from 0 to 1, indicating how much information can be passed through or discarded. Specifically, first, a sigmoid layer called the "forget gate layer" determines how much information to be discarded from the previous cell state, for example, 0 represents all of the information that would be abandoned; second, a sigmoid layer called the "input gate" combined with a hyperbolic tangent (i.e., an activation function in neural network to push the values to be between −1 and 1) layer created a new cell state; finally, the "output gate" will output determined parts based on the cell state.

In this research, LSTM models were built for temperature and precipitation projections with 31 GCMs. First, the inputs of the LSTM model for temperature contain 31 mean temperatures calculated by the maximum and minimum daily temperatures of the 31 GCMs. The paired dataset between the calculated mean daily temperature of 31 GCMs and the observed daily temperature was obtained from 1961 to 2010. The paired dataset for precipitation prediction was formulated based on the monthly precipitation of 31 GCMs and the monthly observed precipitation from 1961 to 2010. Then, temporal signals were detected, and nonlinearity correlations were developed between the downscaled historical and observation data. The period for training the model was determined to be 40 years from 1961 to 2000, and for testing, it was ten years from 2001 to 2010. The evaluation criteria NSE and R were used to represent the prediction accuracy in the reference period. Finally, the temperature (or precipitation) of the 31 GCMs from 2021 to 2050 was fed into the aforementioned LSTM models during 1961–2010 to predict the corresponding future temperature and precipitation, respectively.

Better climatic projections from 2021 to 2050 would be achieved if the temporal signals between the downscaled data from 31 GCMs and the observed data were detected from 1961 to 2010. Deep learning and remembering through LSTM were used to improve the prediction accuracy using observed and downscaled climate data from 1961 to 2010. Using multi-ensemble GCMs and taking 1961 to 2010 as the reference period, the projection of precipitation and temperature from 2021 to 2050 would propagate outputs based on the memory cell of the LSTM. The precipitation and the temperature from 2021 to 2050 were directly averaged from the 31 GCMs using MMEM.

3.4. CA–Markov model

The CA–Markov model, which is formed by integrating the CA model with the Markov model, was adopted to reflect the dynamics of land use patterns. The CA–Markov model synthesizes the advantages of applying multi-standard evaluation and multi-objective decision support systems to define the transfer rules between land use types.

The Markov model is a stochastic process and optimal control theory method for predicting the types and transfer rates of land use [35]. The land use projections based on Bayes are as follows:

$$C(t+1) = \boldsymbol{P}_{ij} \times C(t) \tag{3}$$

where $C(t)$ and $C(t+1)$ are the states at time t and $t+1$, respectively, and $\boldsymbol{P}_{ij}$ is the shift probability matrix of a status, which can be calculated as follows:

$$\boldsymbol{P}_{ij} = \begin{bmatrix} P_{11} & P_{12} & \cdots & P_{1n} \\ P_{21} & P_{22} & \cdots & P_{2n} \\ \cdots & \cdots & \cdots & \cdots \\ P_{n1} & P_{n2} & \cdots & P_{nn} \end{bmatrix} \tag{4}$$

$$0 \le \boldsymbol{P}_{ij} < 1, \sum_{j=1}^{n} P_{ij} = 1 \ (i,j = 1,2,3,\cdots,n)$$

The CA model is a grid dynamics model with discrete-time, space, and state, and can comprehensively consider historical trends, including natural, social, and economic conditions for land use projections. The CA model can be calculated as follows [54]:

$$C(t+1) = f(C(t), D) \tag{5}$$

where t and $t+1$ represent time, C is the set of cellular status, D represents all the cells in a certain neighborhood, and f is the transformation rule of the cellular status. For this research, D contains the influence factors (i.e., elevation, slope, precipitation, temperature, river, road, and population density), f represents the combined rule of each cell in the neighborhood, and $C(t+1)$ represent the land use status at the latter moment, which is affected by the status of the previous moment $C(t)$.

Specifically, the CA–Markov model in the IDRISI software was used to project the long-term land use variation at ten-year intervals of 2025, 2035, and 2045 based on land use maps of 1995, 2005,

and 2015. The detailed processes are as follows: ① calculation of the transfer area matrix and transfer probability matrix of land use types in ARB from 1995 to 2005 and 2005 to 2015; ② selection of natural factors such as elevation, slope, precipitation, temperature, river, and human factors of road and population density as driving factors for land use projection. The MCE and LogisticReg in the module were used to create transition suitability images for each land use type. ③ Based on the spatial distribution and driving factors in 1995 and 2005, the spatial variation of land use for 2015 was simulated, and the actual interpretation data for 2015 were used to verify the simulation results to ensure the reliability of the model. ④ Based on the links between the change and various driving factors, three sets of land use projections for 2025, 2035, and 2045 were projected using three methods.

4. Results and discussion

4.1. Performance of MIKE SHE

The DEM, land use map, soil data, rainfall, wind speed, sunshine duration, and daily maximum and minimum temperatures were used to calibrate the MIKE SHE. The daily streamflow at the watershed outlet was compared with the measured data to assess the model performance under climatic changes. First, MIKE SHE was calibrated during the calibration period (1977–1983) and was validated during the validation period (1984–1986) with data from the daily streamflow at the Wantan station and the 1980 land use map. The model was further validated from 2006 to 2007 using the 2005 land use map (Fig. 3). For the daily simulation, the *R* and the NSE values were 0.85 and 0.72 in the calibration period, 0.87 and 0.73 in the first validation period, and 0.84 and 0.70 in the second validation period, respectively. There was no obvious systematic shift of the relevant points in each period and there were consistent trends, indicating that the Wantan hydrologic station has good consistency for the watershed streamflow. The *R* and NSE values in the calibration period were 0.88 and 0.79, respectively, compared to the monthly streamflow, which was 0.86 and 0.74. The results suggest that MIKE SHE can effectively simulate daily streamflow of ARB. The simulation effect of the monthly scale is better than that of the daily scale, which shows good applicability in mountainous areas as a whole.

We can see from Fig. 3 that the streamflow during spring and winter was relatively small, while it was relatively large during the summer and autumn. From the peak simulation, the simulated value was smaller than the observed value at a certain time. The hydrologic model did not perform well during the second validation period as there were changes in the input vegetation types, illustrating that land use change also affects the hydrological process. Additionally, precipitation and other meteorological data cannot fully represent each calculation unit as the meteorological stations in this study area are sparse, which will have a certain impact on the simulation accuracy of the model.

To validate the applicability of the MIKE SHE model to other hydrologic elements, the actual ET from 1977 to 1986 was simulated and translated into the average value of the study area. The annual mean actual ET was approximately 580–720 $mm{\cdot}a^{-1}$ in the study area, which was consistent with the range of the latest research from the National Tibetan Plateau Data Center, indicating that the actual ET in the southwest river basin (including the Yangtze River) should be significantly higher than 400 $mm{\cdot}a^{-1}$ [55]. The actual ET from 2021 to 2050 will be further analyzed and discussed in the following sections.

4.2. Performance of multi-ensemble GCMs for climate projection

The future climatic conditions were obtained from 31 GCMs using the LSTM and MMEM methods under scenarios of RCP4.5 and RCP8.5, from 2021 to 2050. The downscaled historical data and measured climate data for the period from 1961 to 2000 were used to train the model, whereas data from the period of 2001 to 2010 were used to test the model performance. Table 4 shows the daily temperature and monthly precipitation of meteorological stations from 1961 to 2010 using the two methods. The coefficients of *R* and NSE suggest that the LSTM method has a strong ability for an ensemble of GCMs and can better reflect the daily temperature in the ARB over the reference period. However, certain extreme values still existed that could not be captured perfectly. As 90% of the daily precipitation was zero or extremely low, the LSTM could not predict the extreme values well for capturing most of the data. Certain studies have also indicated that it is usually difficult for RNNs to predict high floating and low regular data impeccably, and daily precipitation has irregular changes and large fluctuations [56]. Thus, daily precipitation with large fluctuations was transformed into monthly precipitation to eliminate zero values, and the results suggested that the LSTM had a strong ability to project monthly precipitation. Furthermore, the coefficients of *R* and NSE indicate that the projected monthly precipitation has a better performance than the daily temperature.

The performance of the LSTM method was evaluated by comparing the projections to the observed precipitation, and it was found that the dataset projected from 31 GCMs of the LSTM method can fit better than the MMEM method (Fig. 4). The monthly average precipitation and daily temperature from the LSTM projection had a stronger correlation with the observed data

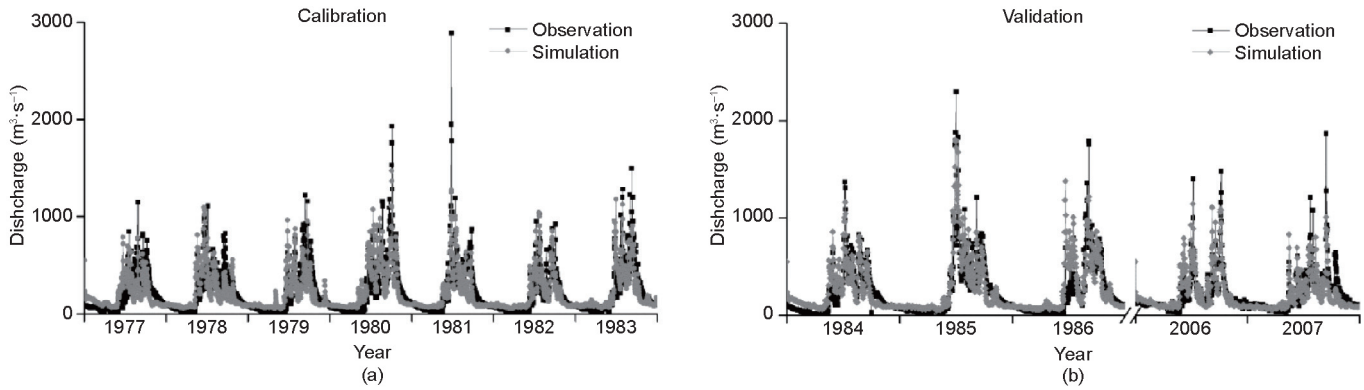

Fig. 3. MIKE SHE simulated and observed daily streamflow at Wantan station during (a) the calibration period (1977–1983) and (b) the validation period (1984–1986 and 2006–2007).

as a whole and could better project the temperature and precipitation over the reference period. For the multi-year monthly precipitation and temperature of Xichang, the precipitation and temperature curves estimated by MMEM were closer to the observations, especially from May to September. However, for monthly precipitation and temperature from 1961 to 2010, the coefficients of *R* and NSE indicate that the climate data estimated by LSTM have a better performance than MMEM at the three stations. The advanced deep learning method of LSTM proved to be more efficient at dealing with temporal signals than the conventional average method of MMEM.

4.3. Future climate projections

Considering the historical period (1961–2010) as the baseline period, the trend of temperature variation in the time period 2021 to 2050 was analyzed using the LSTM and MMEM methods (Fig. 5). Therefore, four sets of climate change scenarios were generated for the influence study from 2021 to 2050 (i.e., RCP4.5_L, RCP8.5_L, RCP4.5_M, and RCP8.5_M). Different variation trends were observed under different ensemble methods from the perspective of the monthly average temperature. The projected values from the LSTM in different scenarios were generally higher than the historical values from October to April, but lower from May to September. The temperature from the MMEM value was higher in the meteorological stations of Mianning and Xichang, but lower in the Miyi station compared to the historical temperature. It also showed different levels of the increasing trend under the two greenhouse emission scenarios of RCP4.5 and RCP8.5, of which the latter had a slightly higher temperature. For the Mianning and Xichang stations, the average annual temperature under RCP4.5 and RCP8.5 projected from LSTM both increased compared with the historical period (1961–2010), and the latter increased approximately 1.4 °C than the former, which is consistent with the results predicted in the IPCC5 report. The increase in watershed temperature will inevitably lead to the rapid melting of glaciers and snow in the ARB headwaters, and a change in the runoff generation mechanism, which will bring new opportunities and challenges to local water resource management and use.

Fig. 6 illustrates the changing trend of projected monthly average precipitation in the future period (2021–2050) under two scenarios (RCP4.5 and RCP8.5) from the MMEM and LSTM values. The precipitation projected from the LSTM was higher than the MMEM at the Mianning and Xichang stations. For the future period (2021–2050), the monthly precipitation under multiple scenarios fluctuated significantly compared to the historical precipitation from May to September, while changing minutely in the other months. The results also indicate that the average annual precipitation

Table 4
Accuracy test of daily temperature and monthly precipitation projection at the three meteorological stations from 1961 to 2010.

Station	Period	Temperature				Precipitation			
		LSTM		MMEM		LSTM		MMEM	
		R	NSE	*R*	NSE	*R*	NSE	*R*	NSE
Mianning	1961–2000	0.89	0.79	0.84	0.69	0.92	0.83	0.76	0.76
	2000–2010	0.85	0.72	0.83	0.68	0.90	0.79	0.82	0.80
Xichang	1961–2000	0.88	0.76	0.81	0.65	0.92	0.84	0.74	0.74
	2000–2010	0.81	0.64	0.79	0.62	0.89	0.76	0.79	0.75
Miyi	1961–2000	0.86	0.73	0.82	0.66	0.92	0.84	0.71	0.71
	2000–2010	0.84	0.71	0.81	0.65	0.88	0.76	0.76	0.74

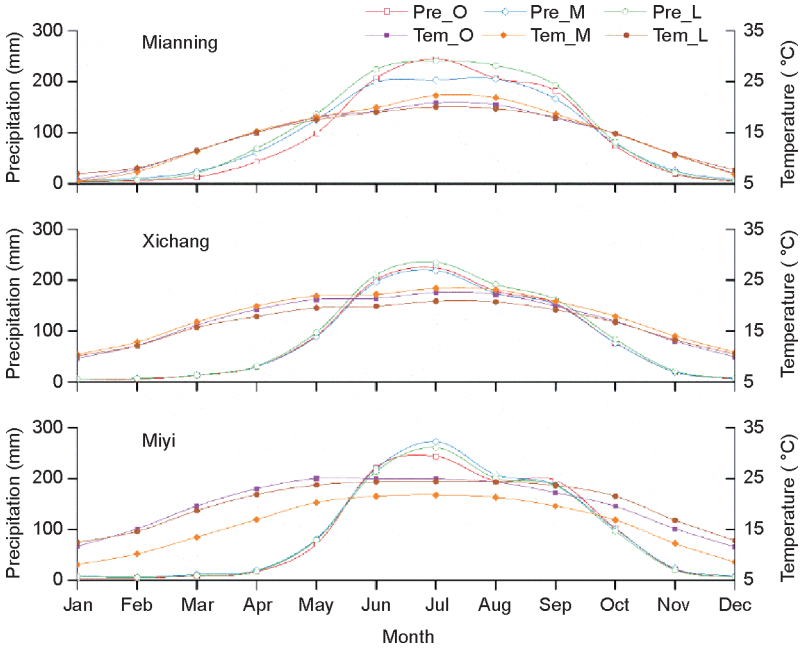

Fig. 4. Multi-year monthly average precipitation and temperature obtained from MMEM and LSTM method (1961–2010). Pre_O: observed precipitation; Pre_M: precipitation projected by MMEM; Pre_L: precipitation projected by LSTM; Tem_O: observed temperature; Tem_M: temperature projected by MMEM; Tem_L: temperature projected by LSTM.

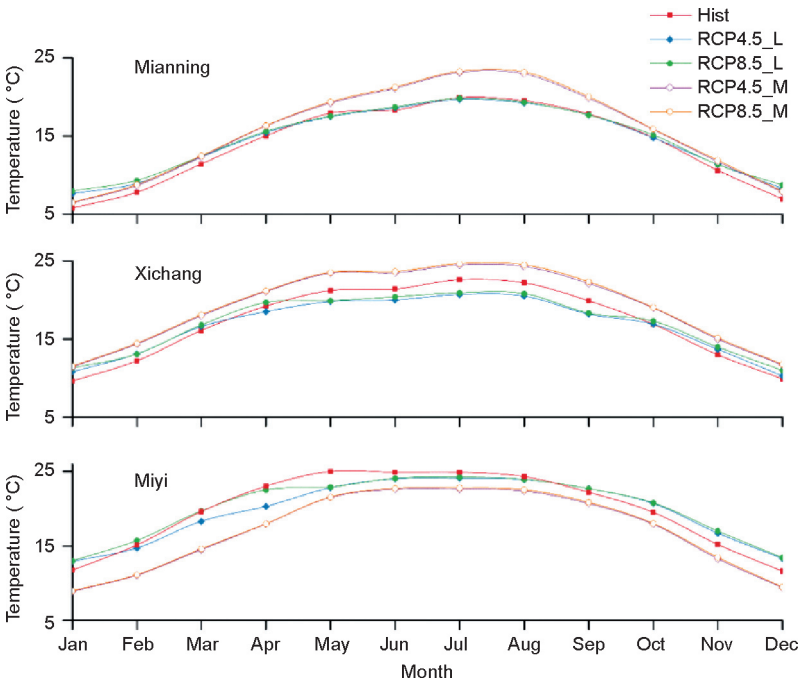

Fig. 5. Monthly average temperature for projected period (2021–2050). Hist: historical period from 1961 to 2010; RCP4.5_L: RCP4.5 projected from LSTM; RCP8.5_L: RCP8.5 projected from LSTM; RCP4.5_M: RCP4.5 projected from MMEM; RCP8.5_M: RCP8.5 projected from MMEM.

under RCP4.5 and RCP8.5 increased relative to the historical period, and the former had an increase of 1.9 mm, especially from June to October.

4.4. Land use projections

The land use during the years 1980, 1995, 2005, and 2015 was classified into five major types, including cropland, forest, grassland, water, and built-up land (Table 5). Specifically, according to the available remote sensing image data, the 1980 land use map in the study area was acquired, and was adopted for calibration during the calibration period (1977–1983) and for validation during the validation period (1984–1986). We mainly obtained the future land use projections based on the land use data from 1995, 2005, and 2015 with transition matrix per decade; thus, the changes from 1980 to 1985 had little influence on land use projections from 2021 to 2050. As presented in Table 5, the dominant land use was forest, followed by cropland and grassland in ARB. This demonstrated that the land use in different types of cropland have sustained reductions over the past

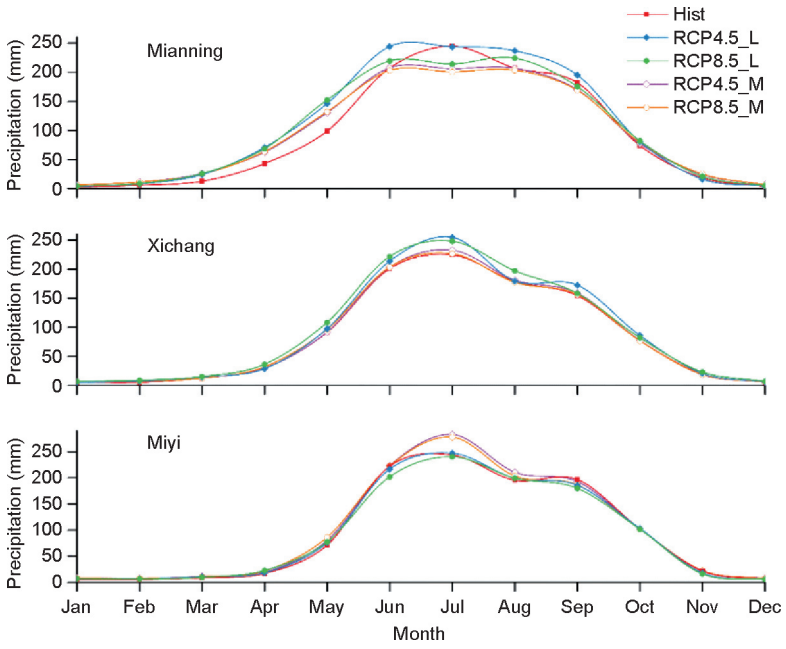

Fig. 6. Monthly average precipitation for the projected period (2021–2050).

decades, which may be attributed to national conservation programs such as the "Grain for Green Project" since the 1990s. The change in the watershed may have been caused by the construction and operation of the Daqiao reservoir in the upper basin since the 1990s and may have been affected by water conservancy projects.

With a comprehensive consideration of the driving factors of land use change, the elevation, slope, precipitation, temperature, river, road, and population density were selected to generate transition suitability images. The representative modules of MCE and LogisticReg combined with the CA–Markov model were adopted to evaluate the relationship between the land use and the driving factors for three sets of land use projections. To test the accuracy of the CA–Markov model's prediction of the quantity and spatial distribution for each land type, the land use of 2015 was projected based on the land use data of 1995 and 2005. The Crosstab module in IDRISI software was used to compare three sets of projections and actual land use maps, the kappa coefficients obtained were 0.96, 0.89, and 0.91, respectively. The results indicate that the CA–Markov model is a dependable estimator and can be used to conduct future land use prediction simulations.

Because of the satisfaction of the calibrated module for 2015, three Markov-based modules (i.e., scenario 1 from MCE; scenario 2 from LogisticReg; scenario 3 from Markov; Fig. 7) were executed to project the land use change of 2025, 2035, and 2045; each land use projection represents the land use map of ten years (i.e., 2025 represents the period of 2021–2030; 2035 represents the period of 2031–2040; and 2045 represents the period of 2041–2050). As can be seen in Fig. 7, the forest area is the largest, followed by cropland and grassland. Built-up land has generally expanded in three scenarios, mainly concentrated in the residential and industrial areas along with the transportation land, especially for the midstream and downstream. The primary trend was the conversion from natural land type to artificial land use type, which seems reasonably feasible to happen because of the regional economic development, increase in population, and other factors. There is no specific methodology to assess the results, and all the future scenarios can occur as no evidence of future conditions exists. As land use varies and spatial variation becomes more complex, it is necessary to strengthen the protection of cropland, forest, and water bodies for the rational use of land.

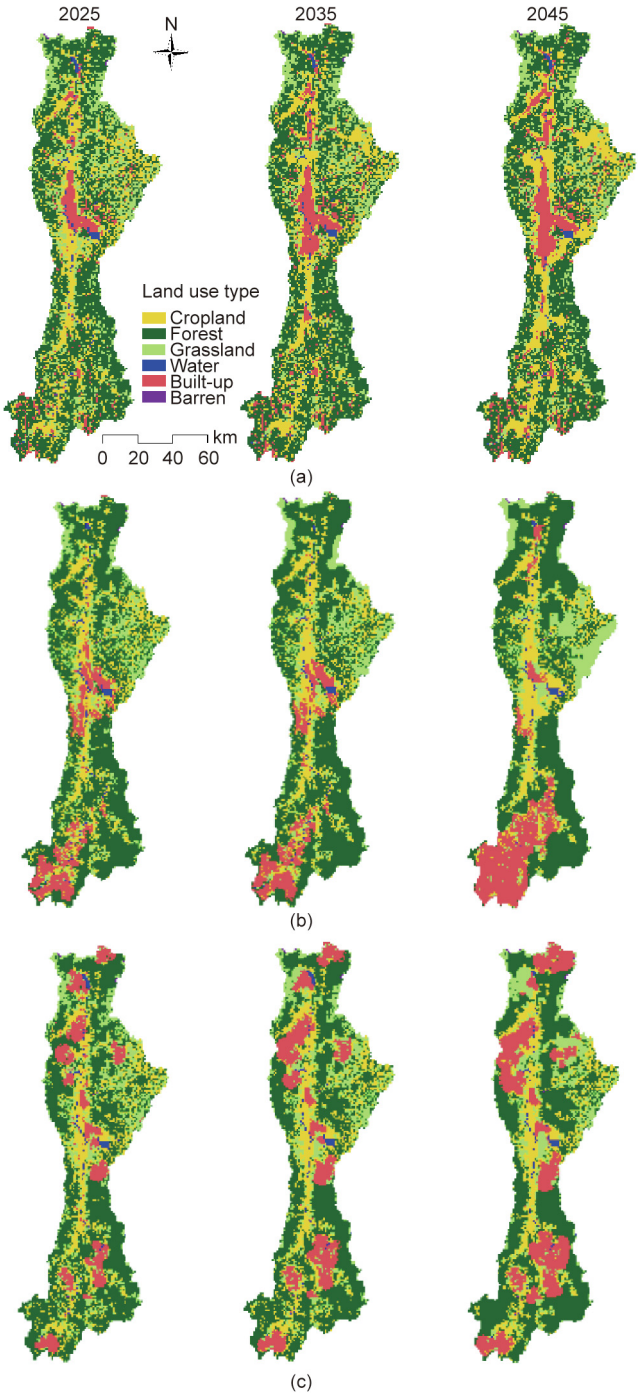

Fig. 7. Three scenarios of land use map projections in 2025, 2035, and 2045. (a) MCE method; (b) LogisticReg method; (c) Markov method.

4.5. Evaluation of hydrologic responses

4.5.1. Streamflow variation to climate and land use changes

Subsequently, based on the above four sets of climate projections and three sets of land use projections, the MIKE SHE model was used to assess the hydrological process in the corresponding period. Cross combination of 12 scenarios were used as inputs to project the process and the trend of streamflow as well as the temporal and spatial variability of the actual ET under climate and land use variations, respectively. The simulated average annual stream-

Table 5
Various land use types and changing rates over 1980–2015 in the watershed.

Type	Land-use area (km^2)					Change rate (%)	
	1980	1995	2005	2015	1980–1995	1995–2005	2005–2015
Cropland	2673	2661	2636	2613	−0.45	−0.94	−0.87
Forest	5990	5978	5978	6003	−0.20	0	0.42
Grassland	2233	2248	2254	2225	0.67	0.27	−1.29
Water	110	112	128	127	1.82	14.29	−0.78
Built-up	57	64	67	95	12.28	4.69	41.79

flow under different scenarios is illustrated in Fig. 8. The streamflow with climate projections from LSTM was higher than that from MMEM. We can see that there was no obvious change in the streamflow under the three land use projections, but it was more sensitive to changes in climate variables. The climatic change is the principal cause of streamflow variations during the historical period, which is consistent with previous research. From the perspective of the multi-year average discharge, the simulated value under the RCP4.5 scenario was higher than that under the RCP8.5, particularly for the period from 2031 to 2040. Even though there was no significant difference in temperature under RCP4.5 and RCP8.5, the future streamflow of the former was higher because of precipitation variations. As precipitation had a great influence on the hydrologic change, the streamflow prediction of low precipitation projections from MMEM was much lower than that from LSTM. We can conclude that the annual runoff increased significantly with an increase in precipitation and decreased with an increase in temperature.

To further analyze the multi-year monthly average distribution of future streamflow variations, box–whisker plots of the change rate under RCP4.5 and RCP8.5 in the future period (2021–2050) were compared with the baseline period (1977–1986) (Fig. 9). The monthly streamflow had an obvious increase from January to April, while it had a dramatic decline from August to November. The reason for the significant increase may be because of the slight increase in temperature, which will inevitably lead to the melting of glaciers and snow in the headwater of ARB. As illustrated in Fig. 9, there was a higher variation in the monthly flows from May to September than in the other months, which indicates a higher uncertainty in the streamflow predictions. Two reasons can illustrate the slight decreasing trend in streamflow under different emission scenarios for the flood period. First, the calibrated hydrologic model did not perform well for the peak value in the flood period because of the deep slopes, valleys, and geographical conditions. Second, although the precipitation had a slight increase during this period, the hydrologic process may be affected by other factors, such as the increased temperature, surface type, cloud cover, sunshine hours, and wind speed. Runoff is likely to increase in the rainy season, especially from May to August; therefore, attention should be paid to prevent the occurrence of flood disasters. The runoff is likely to increase in the dry season compared with the reference period, especially from February to April, while a decrease in runoff during November indicates an increased risk of drought.

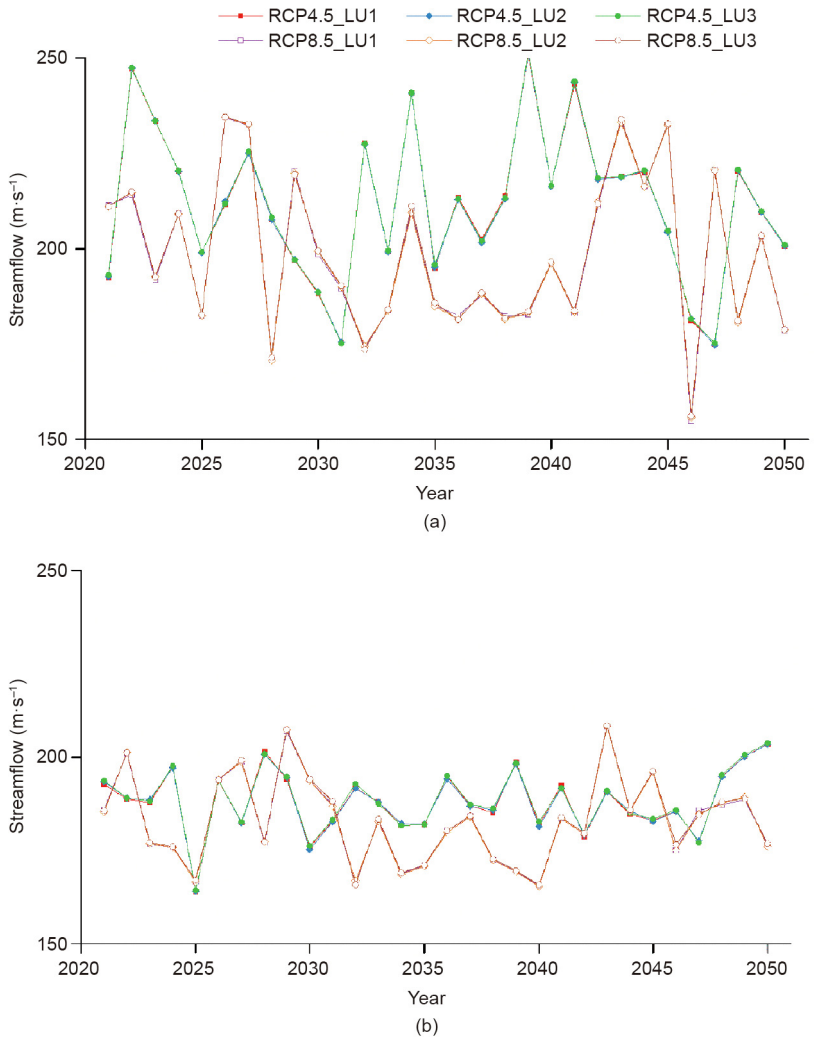

Fig. 8. Streamflow under different scenarios in the future (2021–2050). (a) Climate change projected from LSTM; (b) climate change projected from MMEM. LU1, LU2, and LU3: three land use scenarios.

4.5.2. Temporal and spatial variability of actual ET

For a better assessment of the hydrologic process under changing conditions, an analysis of actual ET was conducted. For this study, the temporal and spatial actual ET was acquired from the output result of MIKE SHE using the two-layer unsaturated zone/evapotranspiration (UZ/ET) model based on a formulation presented by Yan and Smith [57]. Fig. 10 illustrates the spatial variability of the actual annual ET for different climate and land use scenarios. For the simulation results of MIKE SHE, dynamic changes in the actual ET under two climate scenarios and three land use scenarios from 2021 to 2050 were presented compared to the reference period (1977–1986). The actual ET increased with an increase in temperature, and the increase under RCP8.5 (Figs. 10(c) and (d)) was higher than that under RCP4.5 (Figs. 10(a) and (b)), owing to the higher temperature. The actual ET was more sensitive to climate variation than to land use variation according to the influence study.

Fig. 11 illustrates the comparison of streamflow and actual mean ET per decade for each of these scenarios. The annual average streamflow under RCP4.5 was higher than that under RCP 8.5, while the actual ET exhibited a consistent variation trend under different scenarios except for the first land use scenarios under RCP8.5. The components for water balance include precipitation, canopy interception, surface runoff, unsaturated and saturated flow, and so forth. Clearly, precipitation is closely related to the changes in streamflow and the actual ET. Moreover, the increase in temperature can influence ET and reduce canopy resistance in a certain temperature range, of which soil moisture in arid and semi-arid areas positively impacts the actual ET [11]. There was no consistent or opposite correlation between the actual ET and the streamflow, which may be attributed to the uncertainties of future climate and land use projections, as well as the complex topographic conditions.

5. Conclusions

This research revealed the influences of climatic and land use changes on the hydrological process in the dry–warm valley of the Anning River watershed. To address the uncertainty issue that arises from a single GCM, multi-ensemble GCMs using an advanced method of LSTM and a traditional method of MMEM were used in this study to obtain four climatic projections. Three sets of land use projections were generated using a comprehensive consideration of driving factors such as elevation, slope, precipitation, temperature, river, road, and population density. With the constraints of data availability and the large-scale heterogeneity of mountainous areas, this study evaluates the dynamic variation condition and range of hydrologic processes in ARB under complex changing conditions.

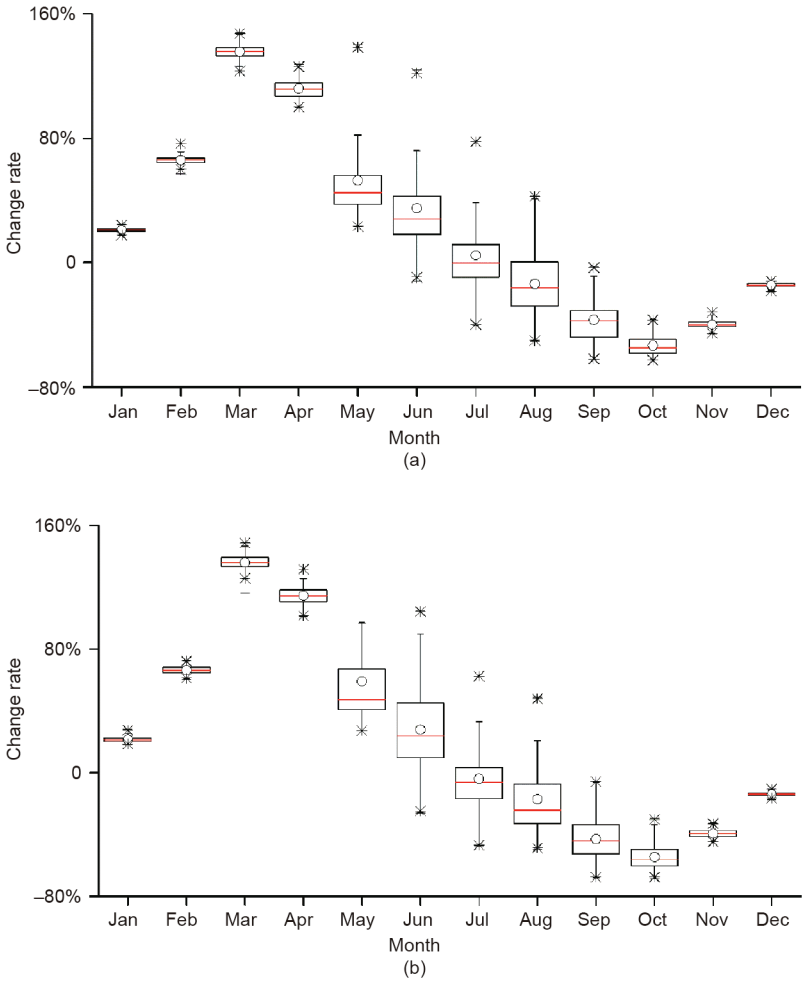

Fig. 9. Projected change of streamflow at the monthly scale in the future period (2021–2050) compared with the baseline period (1977–1986). (a) RCP4.5 scenario; (b) RCP8.5 scenario.

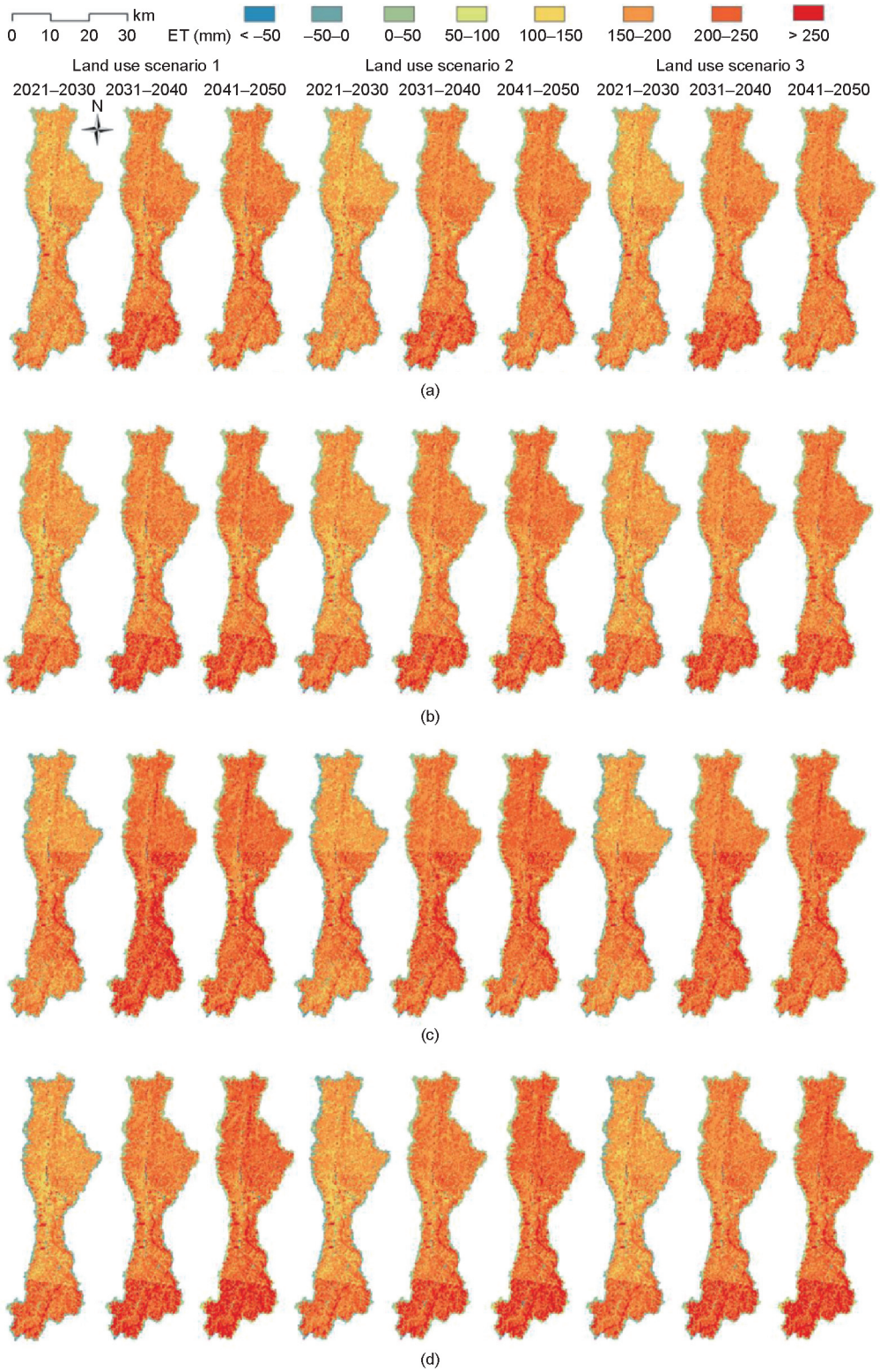

Fig. 10. Spatial variability of annual average ET in 2021–2030, 2031–2040, and 2041–2050 compared with the baseline period of 1977–1986 under RCP4.5 and RCP8.5. (a) climate data projected from LSTM under RCP4.5; (b) climate data projected from MMEM under RCP4.5; (c) climate data projected from LSTM under RCP8.5; (d) climate data projected from MMEM under RCP8.5.

The results showed that the hydrologic model could be effectively applied to streamflow simulation in the dry–warm valley of the ARB. The LSTM method had a better performance for daily temperature and monthly precipitation projections than the traditional MMEM method. However, it was difficult for the LSTM to predict daily precipitation with zero values. The future

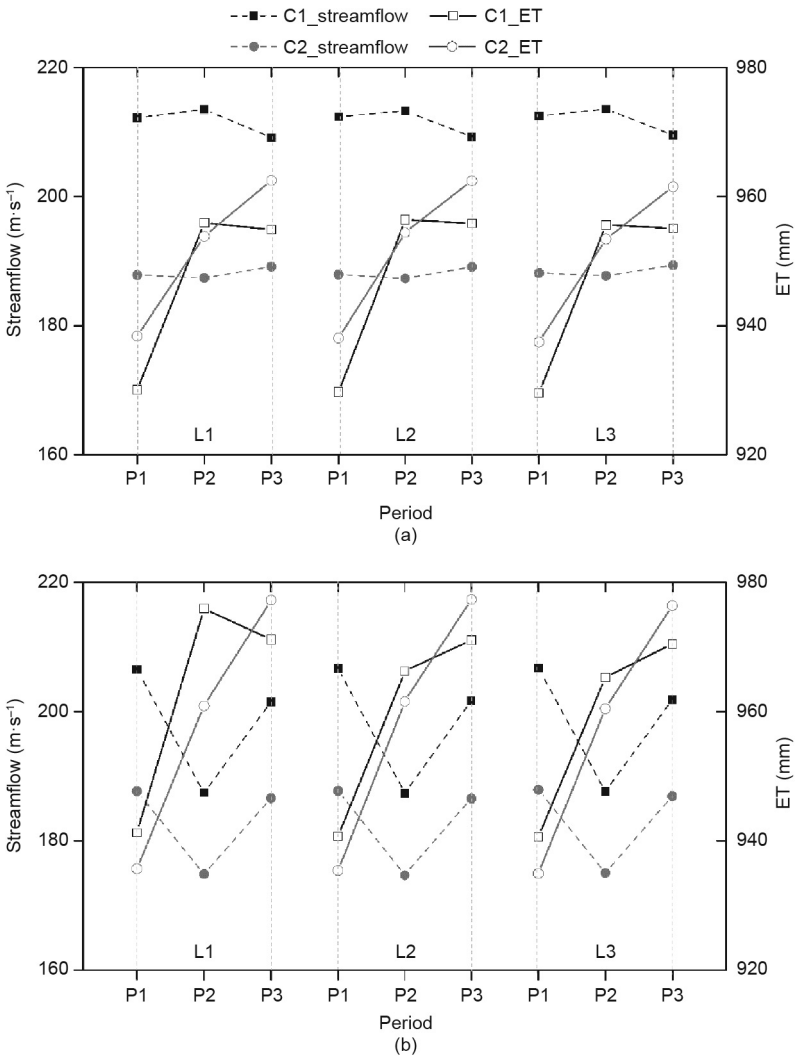

Fig. 11. Comparison of streamflow and actual mean ET per decade. (a) RCP4.5; (b) RCP8.5. C1 and C2: two climate scenarios; L1, L2, and L3: three land use scenarios; P1, P2, and P3: 2021–2030, 2031–2040, and 2041–2050, respectively.

temperature projection under RCP8.5 was slightly higher than that under RCP4.5, while the precipitation projection was slightly lower from June to October. The annual streamflow increased significantly with an increase in precipitation and decreased with an increase in temperature. Runoff and actual ET are more sensitive to climate change than land use changes. Runoff is likely to increase in the rainy season from May to August and decrease during the dry season of November. The actual ET increased with an increase in temperature and had a higher increase under RCP8.5. In future changing environment, effective measures should be taken to deal with flood disasters from May to August, and drought disasters in the dry season, especially in November. As an essential branch of the upper Yangtze River with a fragile ecological environment, it is essential to investigate complicated spatial and temporal variability and stochastic hydrologic processes for complex terrain regions. Consequently, this work could provide an effective guidance for dealing with the risk of flooding and drought in a changing environment, contributing to the sustainable development of the upper Yangtze River's local and downstream areas.

The changing environment presents new challenges to water resources and environmentally sustainable development for the eco-fragile and downstream regions. A dynamic hydrologic model with more updated parameters is expected to explore the complex and uncertain future changing environment.

Acknowledgments

This study was supported by the National Key Research Program of China (2016YFC0502209), Beijing Municipal Natural Science Foundation (JQ18028), and the National Natural Science Foundation of China (51879007 and U20A20117). We acknowledge the modeling groups in making the available CMIP5 multi-model dataset and AGRIVY for providing the data for this study. The authors would also like to express their gratitude to the editor and reviewers for their suggestions to improve the manuscript and references.

Compliance with ethics guidelines

Congcong Li, Yanpeng Cai, Zhong Li, Qianqian Zhang, Lian Sun, Xinyi Li, and Pengxiao Zhou declare that they have no conflict of interest or financial conflicts to disclose.

References

[1] Basheer AK, Lu H, Omer A, Ali AB, Abdelgader AMS. Impacts of climate change under CMIP5 RCP scenarios on the streamflow in the Dinder River and ecosystem habitats in Dinder National Park, Sudan. Hydrol Earth Syst Sci 2016;20(4):1331–53.

[2] Setegn SG, Rayner D, Melesse AM, Dargahi B, Srinivasan R. Impact of climate change on the hydroclimatology of Lake Tana Basin, Ethiopia. Water Resour Res 2011;47(4):W04511.

[3] Zipper SC, Motew M, Booth EG, Chen Xi, Qiu J, Kucharik CJ, et al. Continuous separation of landuse and climate effects on the past and future water balance. J Hydrol 2018;565:106–22.

[4] Sunde MG, He HS, Hubbart JA, Urban MA. Integrating downscaled CMIP5 data with a physically based hydrologic model to estimate potential climate change impacts on streamflow processes in a mixed-use watershed. Hydrol Process 2017;31(9):1790–803.

[5] Guo Y, Shen Y. Agricultural water supply/demand changes under projected future climate change in the arid region of northwestern China. J Hydrol 2016;540:257–73.

[6] Wagena MB, Sommerlot A, Abiy AZ, Collick AS, Langan S, Fuka DR, et al. Climate change in the Blue Nile Basin Ethiopia: implications for water resources and sediment transport. Clim Change 2016;139(2):229–43.

[7] Tan Q, Huang GH, Cai YP. Identification of optimal plans for municipal solid waste management in an environment of fuzziness and two-layer randomness. Stochastic Environ Res Risk Assessment 2010;24 (1):147–64.

[8] Dong C, Tan Q, Huang GH, Cai YP. A dual-inexact fuzzy stochastic model for water resources management and non-point source pollution mitigation under multiple uncertainties. Hydrol Earth Syst Sci 2014;18(5):1793–803.

[9] Sun S, Chen H, Ju W, Hua W, Yu M, Yin Y. Assessing the future hydrological cycle in the Xinjiang Basin, China, using a multi-model ensemble and SWAT model. Int J Climatol 2014;34(9):2972–87.

[10] Asong ZE, Khaliq MN, Wheater HS. Projected changes in precipitation and temperature over the Canadian Prairie Provinces using the Generalized Linear Model statistical downscaling approach. J Hydrol 2016;539:429–46.

[11] Huang T, Yu D, Cao Q, Qiao J. Impacts of meteorological factors and landuse pattern on hydrological elements in a semi-arid basin. Sci Total Environ 2019;690:932–43.

[12] Wilby RL, Harris I. A framework for assessing uncertainties in climate change impacts: low-flow scenarios for the River Thames, UK. Water Resour Res 2006;42(2):W02419.

[13] Ahiablame L, Sinha T, Paul M, Ji JH, Rajib A. Streamflow response to potential landuse and climate changes in the James River watershed, Upper Midwest United States. J Hydrol 2017;14:150–66.

[14] Morán-Tejeda E, Zabalza J, Rahman K, Gago-Silva A, López-Moreno JI, Vicente-Serrano S, et al. Hydrological impacts of climate and land-use changes in a mountain watershed: uncertainty estimation based on model comparison. Ecohydrology 2015;8(8):1396–416.

[15] Ji P, Yuan X. High-resolution land surface modeling of hydrological changes over the Sanjiangyuan Region in the Eastern Tibetan Plateau: 2. impact of climate and land cover change. J Adv Model Earth Syst 2018;10 (11):2829–43.

[16] Sun Y, Tian F, Yang L, Hu H. Exploring the spatial variability of contributions from climate variation and change in catchment properties to streamflow decrease in a mesoscale basin by three different methods. J Hydrol 2014;508:170–80.

[17] Merz R, Parajka J, Bloeschl G. Time stability of catchment model parameters: implications for climate impact analyses. Water Resour Res 2011;47:1–17.

[18] Luo J, Wang E, Shen S, Zheng H, Zhang Y. Effects of conditional parameterization on performance of rainfall-runoff model regarding hydrologic non-stationarity. HyPr 2012;26(26):3953–61.

[19] Silberstein RP, Aryal SK, Durrant J, Pearcey M, Braccia M, Charles SP, et al. Climate change and runoff in south-western Australia. J Hydrol 2012;475:441–55.

[20] Kouhestani S, Eslamian SS, Abedi-Koupai J, Besalatpour AA. Projection of climate change impacts on precipitation using soft-computing techniques: a case study in Zayandeh-rud Basin, Iran. Glob Planet Change 2016;144:158–70.

[21] Mehrotra R, Sharma A, Nagesh Kumar D, Reshmidevi TV. Assessing future rainfall projections using multiple GCMs and a multi-site stochastic downscaling model. J Hydrol 2013;488:84–100.

[22] Sehgal V, Lakhanpal A, Maheswaran R, Khosa R, Sridhar V. Application of multi-scale wavelet entropy and multi-resolution Volterra models for climatic downscaling. J Hydrol 2018;556:1078–95.

[23] Tan Q, Huang GH, Wu CZ, Cai YP, Yan XP. Development of an inexact fuzzy robust programming model for integrated evacuation management under uncertainty. J Urban Plann Dev 2009;135(1):39–49.

[24] Tan Q, Huang GH, Cai YP. A superiority-inferiority-based inexact fuzzy stochastic programming approach for solid waste management under uncertainty. Environ Model Asses 2010;15(5):381–96.

[25] Knutti R, Furrer R, Tebaldi C, Cermak J, Meehl GA. Challenges in combining projections from multiple climate models. J Clim 2010;23 (10):2739–58.

[26] Hochreiter S, Schmidhuber J. Long short-term memory. Neural Comput 1997;9 (8):1735–80.

[27] Zhang Q, Wang H, Dong JY, Zhong GQ, Sun X. Prediction of sea surface temperature using long short-term memory. IEEE Geosci Remote Sens Lett 2017;14(10):1745–9.

[28] LeCun Y, Bengio Y, Hinton G. Deep learning. Nature 2015;521(7553):436–44.

[29] Sonkoue D, Monkam D, Fotso-Nguemo TC, Yepdo ZD, Vondou DA. Evaluation and projected changes in daily rainfall characteristics over Central Africa based on a multi-model ensemble mean of CMIP5 simulations. Theor Appl Clim 2019;137(3–4):2167–86.

[30] Rong Q, Zeng J, Su M, Yue W, Xu C, Cai Y. Management optimization of nonpoint source pollution considering the risk of exceeding criteria under uncertainty. Sci Total Environ 2021;758:143659.

[31] Zhu R, Yang L, Liu T, Wen X, Zhang L, Chang Y. Hydrological responses to the future climate change in a data scarce region, northwest China: application of machine learning models. Water 2019;11(8):1–19.

[32] Cai YP, Huang GH, Yang ZF, Tan Q. Identification of optimal strategies for energy management systems planning under multiple uncertainties. Appl Energy 2009;86(4):480–95.

[33] Wang Y, Li X, Zhang Q, Li J, Zhou X. Projections of future land use changes: Multiple scenarios-based impacts analysis on ecosystem services for Wuhan city, China. Ecol Indic 2018;94:430–45.

[34] Hishe S, Bewket W, Nyssen J, Lyimo J. Analysing past landuse land cover change and CA–Markov-based future modelling in the Middle Suluh Valley, northern Ethiopia. Geocarto Int 2020;35(3):225–55.

[35] Yan R, Cai Y, Li C, Wang X, Liu Q. Hydrological responses to climate and landuse changes in a watershed of the Loess Plateau, China. Sustainability 2019;11 (5):1443.

[36] Shao H, Liu M, Shao Q, Sun X, Wu J, Xiang Z, et al. Research on eco-environmental vulnerability evaluation of the Anning River Basin in the upper reaches of the Yangtze River. Environ Earth Sci 2014;72(5):1555–68.

[37] Zhang D, Zhang Q, Qiu J, Bai P, Liang K, Li X. Intensification of hydrological drought due to human activity in the middle reaches of the Yangtze River, China. Sci Total Environ 2018;637–638:1432–42.

[38] Zhang JP, Yang Z, Wang DJ, Zhang XB. Climate change and causes in the Yuanmou dry–hot valley of Yunnan, China. J Arid Environ 2002;51 (1):153–62.

[39] Abbott MB, Bathurst JC, Cunge JA, Oconnell PE, Rasmussen J. An introduction to the European hydrological system—systeme hydrologique europeen, SHE. 1: history and philosophy of a physically-based, distributed modeling system. J Hydrol 1986;87(1–2):45–59.

[40] Zhang Z, Wang S, Sun G, McNulty SG, Zhang H, Li J, et al. Evaluation of the MIKE SHE model for application in the Loess Plateau, China. J Am Water Resour As 2008;44(5):1108–20.

[41] Thompson JR, Sorenson HR, Gavin H, Refsgaard A. Application of the coupled MIKE SHE/MIKE 11 modelling system to a lowland wet grassland in southeast England. J Hydrol 2004;293(1–4):151–79.

[42] Christiaens K, Feyen J. Constraining soil hydraulic parameter and output uncertainty of the distributed hydrological MIKE SHE model using the GLUE framework. Hydrol Process 2002;16(2):373–91.

[43] Ebel BA. Simulated unsaturated flow processes after wildfire and interactions with slope aspect. Water Resour Res 2013;49(12):8090–107.

[44] McMichael CE, Hope AS. Predicting streamflow response to fire-induced landcover change: implications of parameter uncertainty in the MIKE SHE model. J Environ Manage 2007;84(3):245–56.

[45] Stisen S, Jensen KH, Sandholt I, Grimes DIF. A remote sensing driven distributed hydrological model of the Senegal River basin. J Hydrol 2008;354 (1–4):131–48.

[46] Thompson JR. Modelling the impacts of climate change on upland catchments in southwest Scotland using MIKE SHE and the UKCP09 probabilistic projections. Hydrol Res 2012;43(4):507–30.

[47] Wijesekara GN, Farjad B, Gupta A, Qiao Y, Delaney P, Marceau DJ. A comprehensive land-use/hydrological modeling system for scenario simulations in the Elbow River Watershed, Alberta, Canada. Environ Manage 2014;53(2):357–81.

[48] Thompson JR, Green AJ, Kingston DG, Gosling SN. Assessment of uncertainty in river flow projections for the Mekong River using multiple GCMs and hydrological models. J Hydrol 2013;486:1–30.

[49] Guo D, Westra S, Maier HR. An R package for modelling actual, potential and reference evapotranspiration. Environ Model Software 2016;78:216–24.

[50] Wang S, Zhang Z, Sun G, Strauss P, Guo J, Tang Y, et al. Multi-site calibration, validation, and sensitivity analysis of the MIKE SHE Model for a large watershed in northern China. Hydrol Earth Syst Sci 2012;16(12):4621–32.

[51] Wijesekara GN, Gupta A, Valeo C, Hasbani JG, Qiao Y, Delaney P, et al. Assessing the impact of future land-use changes on hydrological processes in the Elbow River watershed in southern Alberta, Canada. J Hydrol 2012;412–413:220–32.

[52] Liu DL, Zuo HP. Statistical downscaling of daily climate variables for climate change impact assessment over New South Wales, Australia. Clim Change 2012;115(3–4):629–66.

[53] Meinshausen M, Smith SJ, Calvin K, Daniel JS, Kainuma MLT, Lamarque JF, et al. The RCP greenhouse gas concentrations and their extensions from 1765 to 2300. Clim Change 2011;109(1–2):213–41.

[54] Wu H, Li Z, Clarke KC, Shi W, Fang L, Lin A, et al. Examining the sensitivity of spatial scale in cellular automata Markov chain simulation of landuse change. Int J Geogr Inf Sci 2019;33(5):1040–61.

[55] Ma N, Szilagyi J, Zhang YS, Liu WB. Complementary-relationship-based modeling of terrestrial evapotranspiration across China during 1982–2012:

validations and spatiotemporal analyses. J Geophys Res-Atmos 2019;124:4326–51.
[56] Li C, Cai Y, Tan Q, Wang X, Li C, Liu Q, et al. An integrated simulation-optimization modeling system for water resources management under coupled impacts of climate and landuse variabilities with priority in ecological protection. Adv Water Resour 2021;154:103986.
[57] Yan J, Smith KR. Simulation of integrated surface water and ground water systems—model formulation. Water Resour Bull 1994;30(5):879–90.